



Analysis of radial flow reformer for fuel cell applications

Wesley A. Teichmiller, Srinivas Palanki*

Department of Chemical & Biomolecular Engineering, University of South Alabama, 307 University Blvd N., Mobile, AL 36688-0002, USA

ARTICLE INFO

Article history:

Received 18 May 2009

Received in revised form 10 August 2009

Accepted 14 August 2009

Available online 28 August 2009

Keywords:

Methane reforming
Radial flow geometry
Hydrogen generation

ABSTRACT

In this paper, the performance of a radial flow reformer is analyzed. Fundamental principles of reaction engineering are utilized to design this reactor where methane is reformed to produce sufficient hydrogen to generate 20 W of power in a fuel cell. It is shown that the radial flow geometry leads to modest pressure drop. The reactor operates at a pressure of 150 kPa, a steam to methane ratio of 3 and an inlet temperature of 848 K and is able to generate sufficient hydrogen for 20 W of power. The heat duty required for the reformer is approximately 43% of the power generated.

© 2009 Elsevier B.V. All rights reserved.

1. Introduction

There is current interest in the development of technologies that provide alternatives to conventional batteries in the 20 W power range. In particular, the development of systems that utilize fuel cells can provide thermodynamic and environmental advantages [4]. Fuel cells can operate for longer durations as compared to batteries and are only limited by the size of the fuel tank for generating power continuously. Furthermore, they have high efficiencies, low emissions, high reliability, quiet operation and easy monitoring capabilities.

Some of the applications identified by the U.S. Army in the 20 W range [13] that could utilize fuel cells are radios (6–7 W), computer displays (3–7 W), sensors (9.5 W), and computers (17–18 W). Furthermore, several unmanned air vehicles such as BATCAM, Hornet and Wasp require about 20 W of power [18]. While the ultimate goal is to use *renewable* resources to produce hydrogen that can be utilized in a fuel cell, in the near-term it is envisioned that reformer technology will be utilized to extract hydrogen of the desired purity from a fossil fuel. This hydrogen will then be used in a fuel cell to generate power at the desired level. Steam reforming of hydrocarbons is an attractive route for the production of hydrogen for use in the generation of power from fuel cells [10] and there has been recent interest in developing chemical systems for generating hydrogen. Micro and meso-scale systems are well suited to small-scale power generation as they enable integration and stacking of the various components (fuel processor, fuel cell and fuel delivery system) into a compact power generating unit. Pattekar and

Kothare [15] fabricated a radial flow micro-packed-bed reactor via deep reactive ion etching that utilizes methanol to generate sufficient hydrogen for a 20 W power application. Kundu et al. [8] developed a serpentine patterned micro-reformer that converts methanol to hydrogen via steam reforming. Chu et al. [3] developed a compact reformer that utilizes natural gas or propane to deliver up to 3 kW of power. Kolb et al. [7] developed a microstructured reactor that produces up to 5 kW of power using iso-octane as a hydrocarbon source for producing hydrogen for mobile auxiliary power units. An exhaustive review of micro-reactors is available in Kundu et al. [9].

While there are a large number of papers on fabrication of small-scale reformers, there are few papers on modeling and analysis of these devices. Most modeling efforts in the literature have focused on modeling micro-reformers based on a channel geometry using structured catalysts. For instance, Zanfir and Gavrilidis [22] studied methane steam reforming in a catalytic plate reactor where reforming and combustion occurred in alternate channels that were 1–4 mm wide. A two dimensional model was developed and the resulting set of partial differential equations were solved numerically for methane conversion and temperature as a function of reactor length. Norton and Vlachos [14] studied combustion characteristics and flame stability via a computation fluid dynamics (CFD) model. Tonkovich et al. [17] utilized a commercial CFD package to analyze methane reforming reactions in a microchannel reactor. Kaisare and Vlachos [6] developed a one dimensional model to study methane and propane reforming in a parallel plate reactor with structured catalysts.

The goal of this paper is to utilize fundamental principles of reaction engineering to design a radial-flow reformer that supplies the necessary amount of hydrogen via steam reforming of methane to a fuel cell for 20 W applications in an attempt to replace less effi-

* Corresponding author.

E-mail address: spalanki@usouthal.edu (S. Palanki).

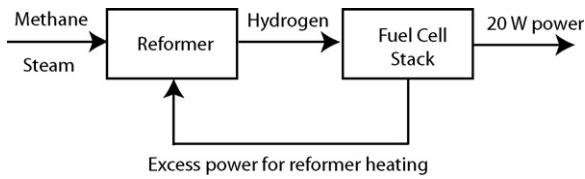
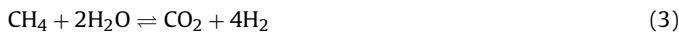


Fig. 1. General schematic of micro-reformer and fuel cell system.

cient batteries. The radial flow geometry is analyzed in this paper because of its potential to reduce pressure drop. The reactor is fed with controlled gas-flow from a renewable fuel tank as opposed to the complete replacement of a battery. A schematic of the process under consideration is shown in Fig. 1.

2. Reaction kinetics

The following chemical reactions occur in the steam reformer:



Xu and Froment [21] developed intrinsic rate expressions for the steam reforming of methane on a Ni/MgO · Al₂O₃ catalyst. These expressions incorporate each chemicals composition/partial pressure, adsorption coefficients, and rate constants. The following rate laws were derived from experimental data:

$$-r_{1,\text{CO}} = \frac{(k_1/P_{\text{H}_2}^{2.5})(P_{\text{CH}_4}P_{\text{H}_2\text{O}} - ((P_{\text{H}_2}^3 P_{\text{CO}})/K_1))}{(1 + K_{\text{CO}}P_{\text{CO}} + K_{\text{H}_2}P_{\text{H}_2} + K_{\text{CH}_4}P_{\text{CH}_4} + K_{\text{H}_2\text{O}}P_{\text{H}_2\text{O}}/P_{\text{H}_2})^2} \quad (4)$$

$$-r_{2,\text{CO}_2} = \frac{(k_2/P_{\text{H}_2})(P_{\text{CO}}P_{\text{H}_2\text{O}} - ((P_{\text{H}_2}P_{\text{CO}_2})/K_2))}{(1 + K_{\text{CO}}P_{\text{CO}} + K_{\text{H}_2}P_{\text{H}_2} + K_{\text{CH}_4}P_{\text{CH}_4} + K_{\text{H}_2\text{O}}P_{\text{H}_2\text{O}}/P_{\text{H}_2})^2} \quad (5)$$

$$-r_{3,\text{CO}_2} = \frac{(k_3/P_{\text{H}_2}^{3.5})(P_{\text{CH}_4}P_{\text{H}_2\text{O}}^2 - ((P_{\text{H}_2}^4 P_{\text{CO}_2})/K_3))}{(1 + K_{\text{CO}}P_{\text{CO}} + K_{\text{H}_2}P_{\text{H}_2} + K_{\text{CH}_4}P_{\text{CH}_4} + K_{\text{H}_2\text{O}}P_{\text{H}_2\text{O}}/P_{\text{H}_2})^2} \quad (6)$$

where $r_{1,\text{CO}}$, r_{2,CO_2} , r_{3,CO_2} are rates of reaction for steam reforming of methane and water gas shift reactions, P_{CH_4} , P_{CO} , P_{O_2} are the partial pressures of methane, carbon monoxide and carbon dioxide, respectively.

3. Reformer modeling and simulation conditions

The reformer is modeled as a radial flow packed bed reactor. The pressure drop is modeled via the Ergun equation [5]. Since the reforming reactions are endothermic, some of the power produced is used to heat the reactor via resistive heating.

The steady-state model equations for each species are given as follows:

$$\frac{dF_{\text{H}_2}}{dz} = (3r_{1,\text{CO}} + r_{2,\text{CO}_2} + 4r_{3,\text{CO}_2})(2\pi zh) \quad (7)$$

$$\frac{dF_{\text{CO}}}{dz} = (r_{1,\text{CO}} - r_{2,\text{CO}_2})(2\pi zh) \quad (8)$$

$$\frac{dF_{\text{CO}_2}}{dz} = (r_{2,\text{CO}_2} + r_{3,\text{CO}_2})(2\pi zh) \quad (9)$$

$$\frac{dF_{\text{CH}_4}}{dz} = (-r_{1,\text{CO}} - r_{3,\text{CO}_2})(2\pi zh) \quad (10)$$

$$\frac{dF_{\text{H}_2\text{O}}}{dz} = (-r_{1,\text{CO}} - r_{2,\text{CO}_2} - 2r_{3,\text{CO}_2})(2\pi zh) \quad (11)$$

where $F_{\text{H}_2\text{O}}$, F_{CO} , F_{H_2} , F_{CH_4} , F_{CO_2} are the molar flow rates of steam, carbon monoxide, hydrogen, methane, and carbon dioxide, respectively, h is the reactor depth and z is the radial dimension of the

reactor. The term, $2\pi zh$ represents the area of cross section of the reactor that is perpendicular to the flow and is a function of the radial direction.

The pressure drop equation is given by:

$$\frac{dP}{dz} = -\frac{G}{\rho D_p} \left(\frac{1-\phi}{\phi^3} \right) \left[\frac{150(1-\phi)\eta_m}{D_p} + 1.75G \right] \quad (12)$$

where P is the reactor pressure, ϕ is the void fraction, D_p is the diameter of the catalyst particle in the reformer, η_m is the viscosity of the gas mixture, ρ is the gas mixture density and G is the superficial mass velocity.

The Ergun equation requires the computation of the gas mixture density, ρ , as well as the gas mixture viscosity, η_m , as a function of reactor radius. The mixture density is estimated by computing the mole average density of the gas mixture at each integration step. Due to the presence of hydrogen in the gas mixture, the mole average method can lead to significant errors in the computation of overall gas mixture viscosity [1]. For this reason, Wilke's method [16] is utilized to estimate the gas viscosity at each integration step as shown below:

$$\eta_m = \frac{\sum_{i=1}^n \frac{y_i \eta_i}{n}}{\sum_{j=1}^n y_j \phi_{ij}} \quad (13)$$

where

$$\phi_{ij} = \frac{[1 + (\eta_i/\eta_j)^{0.5}(M_j/M_i)^{0.25}]^2}{[8(1 + (M_i/M_j))]^{0.5}} \quad (14)$$

In the above equations η_m is the viscosity of the mixture, η_i , y_i , and M_i are the viscosity, mole fraction and molecular weight of pure component i . The pure component viscosity is calculated by the following equation:

$$\eta_i = \frac{(26.69MT)^{0.5}}{\sigma^2 \Omega} \quad (15)$$

where σ is the hard sphere diameter, Ω is the collision integral and T is the temperature. Hard sphere diameters are obtained from [16] and the collision integral is calculated by the following equation:

$$\Omega = \frac{1.16145}{\bar{T}^{0.14874}} + \frac{0.52487}{e^{0.77320\bar{T}}} + \frac{2.16178}{e^{2.4378\bar{T}}} \quad (16)$$

where \bar{T} is the dimensionless temperature given by T/E_k and E_k is the minimum of pair potential energy divided by Boltzmann constant. Minimum of pair potential energy is obtained from Poling et al. [16].

A steady-state energy balance on the reformer leads to the following equation [5]:

$$\frac{dT}{dz} = \frac{(Q + r_{1,\text{CO}}\Delta H_1 + r_{2,\text{CO}_2}\Delta H_2 + r_{3,\text{CO}_2}\Delta H_3)}{(F_{\text{H}_2\text{O}}C_{p_{\text{H}_2\text{O}}} + F_{\text{CO}}C_{p_{\text{CO}}} + F_{\text{H}_2}C_{p_{\text{H}_2}} + F_{\text{CH}_4}C_{p_{\text{CH}_4}} + F_{\text{CO}_2}C_{p_{\text{CO}_2}})} \times (2\pi zh) \quad (17)$$

where T is the reformer temperature, ΔH_i is the heat of reaction for reaction r_i , Q is the heat input to the reactor, and C_{p_j} is the specific heat of species j and is given by:

$$C_{p_j} = \int_{T_0}^T (a + bT + cT^2 + dT^3) dT \quad (18)$$

The constants a , b , c , and d for each species are obtained from Poling et al. [16] and are listed in Table 5.

The above model is developed under the assumption that diffusion effects were negligible. This assumption is verified by calculating the Thiele modulus and the effectiveness factor [5].

Table 1
Parameters for effectiveness factor calculation.

Parameter	Value
v_{CH_4} (cm ³ /mol)	24.42
$v_{\text{H}_2\text{O}}$ (cm ³ /mol)	9.441
M_{CH_4} (g/mol)	16.043
$M_{\text{H}_2\text{O}}$ (g/mol)	18.015
ξ	0.3
χ	4

For this calculation, the catalyst is assumed to be spherical, the methane kinetics represented by Eq. (1) are linearized and the other reactions are ignored. Under these assumptions, the effectiveness factor, η_{eff} can be represented as follows [5]:

$$\eta_{\text{eff}} = \frac{3}{\Phi} \left(\frac{1}{\tanh(\Phi)} - \frac{1}{\Phi} \right) \quad (19)$$

where the Thiele modulus Φ is given by the following expression [5]:

$$\Phi = \frac{D_p}{2} \sqrt{\frac{k}{D_{\text{eff}}}} \quad (20)$$

In the above equation, k is the intrinsic rate constant, and D_{eff} is the effective diffusion coefficient, which is found from:

$$D_{\text{eff}} = D_{\text{methane-steam}} \frac{\xi}{\chi} \quad (21)$$

where $D_{\text{methane-steam}}$ is the diffusion coefficient between methane and steam, ξ is the particle porosity and χ is the tortuosity. The diffusion coefficient was found from the Fuller equation as follows [11]:

$$D_{\text{methane-steam}} = \frac{0.1013T^{1.75}((1/M_{\text{CH}_4}) + (1/M_{\text{H}_2\text{O}}))^{0.5}}{P(v_{\text{CH}_4}^{0.33} + v_{\text{H}_2\text{O}}^{0.33})^2} \quad (22)$$

Table 1 shows the parameters used in the computation of the effectiveness factor. Using Eqs. (19)–(22), it is determined that the Thiele modulus for the system under consideration is 0.029, which results in an effectiveness factor of unity. This indicates that pore diffusion effects are negligible for the simulation conditions studied in the reformer. Since the reactants and products are in gas phase on a porous catalyst, film mass transfer is negligible as well [11] and the operating regime is due to reaction kinetics rather than mass transfer.

4. Fuel cell stack design

The relation between hydrogen flow rate, current, and the number of cells is given by Larminie and Dicks [10]:

$$I = \frac{2F\epsilon F_{\text{H}_2}}{n} \quad (23)$$

where I is the current, F is Faraday's constant, F_{H_2} is the molar flow rate of hydrogen entering the fuel cell stack, ϵ is an efficiency factor and n is the number of cells in the fuel cell stack.

The desired power generated by the fuel cell stack is computed from:

$$P = VI \quad (24)$$

where P is the power and V is the voltage.

The polarization curve shown in Fig. 2 is utilized to model the relation between voltage and power density [2]. Fuel cell stack parameters are shown in Table 2.

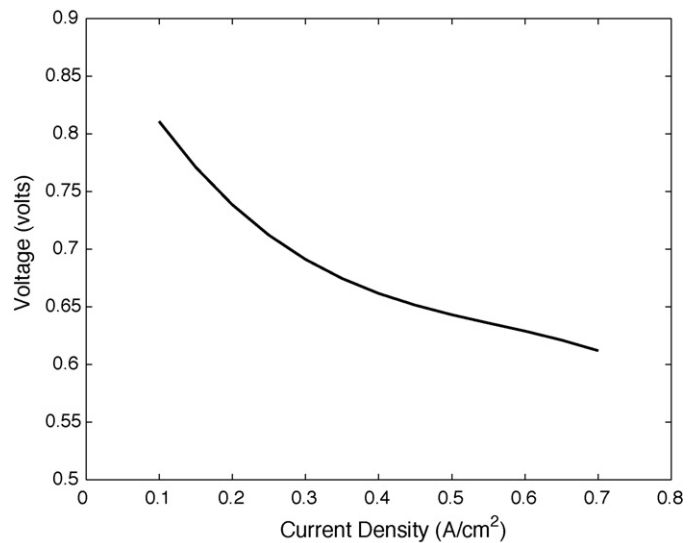


Fig. 2. Polarization curve.

Table 2
Fuel cell stack parameters.

Number of cells, n	20
Area of cross section of each cell, A (cm ²)	12.4
Efficiency factor, ϵ	0.80
Faraday's constant, F (C/mol)	96,487

Table 3
Kinetic and thermodynamic parameters.

Parameter	Value
k_1 ((mol atm ^{0.5})/(m ³ min))	$9.886 \times 10^{16} \exp(-240100/(RT))$
k_2 (mol/(atm m ³ min))	$4.665 \times 10^7 \exp(-67130/(RT))$
k_3 ((mol atm ^{0.5})/(m ³ min))	$2.386 \times 10^{16} \exp(-243900/(RT))$
K_1 (atm ²)	$\exp(29.3014 - 26248.4/T)$
K_2	$\exp(-4.35369 + 4593.17/T)$
K_3 (atm ²)	$\exp(25.225 - 21825.28/T)$
K_{CO} (atm ⁻¹)	$8.339 \times 10^{-5} \exp(70650/(RT))$
K_{H_2} (atm ⁻¹)	$6.209 \times 10^{-9} \exp(82900/(RT))$
K_{CH_4} (atm ⁻¹)	$6.738 \times 10^{-4} \exp(38280/(RT))$
$K_{\text{H}_2\text{O}}$	$1.770 \times 10^5 \exp(-88680/(RT))$

5. Simulation results and discussion

The design equations described by Eqs. (7)–(12) were integrated numerically in MATLAB using the stiff ordinary differential equations routine *ode15s*. Table 3 lists the values of the thermodynamic and kinetic parameters, Table 4 lists the reactor parameters, and Table 5 lists the parameters for density, viscosity and energy balance used in simulation studies in this research. Heat of formation and specific heat for each species was used to compute the heats of reaction. The flow rate of methane to the reformer was fixed at 5×10^{-4} mol/s. The steam to methane ratio was kept at 3 to avoid coking in the reactor [22] and the inlet pressure was kept at 150 kPa. The kinetics developed by Xu and Froment [21]

Table 4
Reactor parameters.

Parameter	Value
Catalyst particle diameter, D_p (m)	0.0001
Catalyst density, ρ (kg/m ³)	2835
Void fraction, ϕ	0.38
Reactor inner radius, r_i (m)	0.005
Reactor outer radius, r_o (m)	0.04
Reactor depth (radial flow), h (m)	0.01

Table 5
Parameters for density, viscosity and energy balance calculation.

Component	H ₂	CO	CO ₂	CH ₄	H ₂ O
Density (g/mol)	2.016	28.01	44.01	16.043	18.015
Hard sphere dia. (Å)	2.827	3.69	3.941	3.758	2.641
Pair Pot./Boltzman const. (K)	59.7	91.7	195.2	148.6	809.1
Heat of formation (kJ/mol)	0	-110.52	-393.5	-74.85	-241.83
Heat capacity constants					
<i>a</i>	0.02884	0.02895	0.03611	0.03431	0.03346
<i>b</i>	7.65×10^{-8}	4.11×10^{-6}	4.23×10^{-5}	5.47×10^{-5}	6.88×10^{-6}
<i>c</i>	3.29×10^{-9}	3.55×10^{-9}	-2.90×10^{-8}	3.66×10^{-9}	7.60×10^{-9}
<i>d</i>	-8.70×10^{-13}	-2.22×10^{-12}	7.46×10^{-12}	-1.10×10^{-11}	-3.60×10^{-12}

Table 6
Relation between flow rate of hydrogen and the power produced by fuel cell.

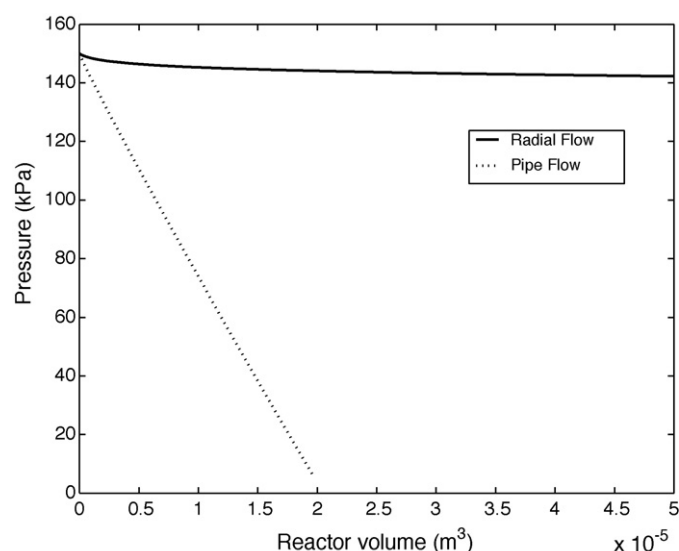
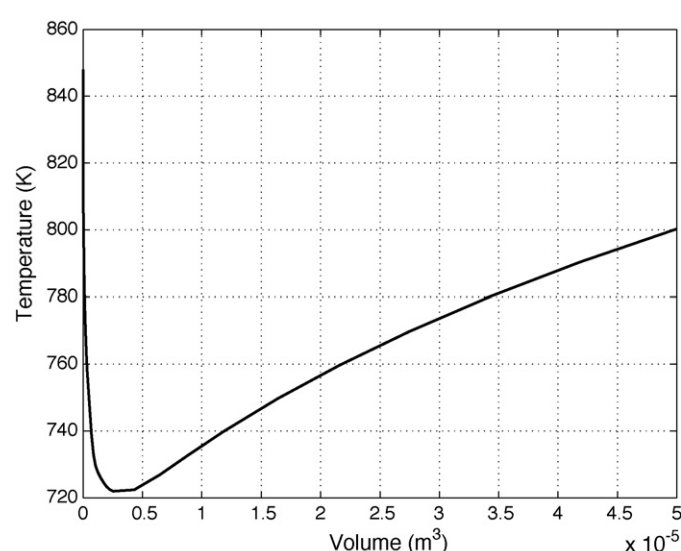
Power supplied (W)	Hydrogen flow rate (mol/s)	Power produced (W)	Net power (W)
0	0.995×10^{-4}	12.99	12.99
5	1.644×10^{-4}	20.52	15.52
10	2.356×10^{-4}	28.13	18.13
15	3.066×10^{-4}	35.21	20.21
20	3.766×10^{-4}	41.84	21.84
25	4.454×10^{-4}	48.13	23.13

were based on experiments run between 778 and 848 K. Since the methane reforming reaction is endothermic, we used an inlet temperature of 848 K (the highest possible temperature for which the kinetic expressions were experimentally verified). The rate kinetics represented by Eqs. (4)–(6) have a term in the denominator where a division by the partial pressure of hydrogen occurs. To avoid numerical integration problems at the reformer inlet, it was assumed that a trace amount of hydrogen (1×10^{-8} mol/s) enters the reformer. The hydrogen flow rate coming out of the reformer was used in Eq. (23) to compute the current generated by the fuel cell. The polarization curve represented by Fig. 2 is used to compute the corresponding voltage and Eq. (24) was used to compute the total power generated. The energy balance represented by Eq. (17) assumes that the reformer is heated via resistive heating and this power is supplied by the fuel cell. Table 6 shows the relation between the power supplied to the reformer, the flow rate of hydrogen produced and the corresponding power produced by the fuel cell. In each of these simulations, conversion of methane was less than 10% and was significantly below equilibrium conversion. It is observed that if the reformer is operated adiabatically, the net

power produced is only 13 W, which is below the design specification of 20 W. As more power is provided to the reformer for heating, more hydrogen is produced due to a faster rate of reaction. However, the increase in power is off-set by the increased heating demand of the reformer. When 15 W is supplied to the reformer, the fuel cell produces a total of 35 W, which translates to a net power gain of 20 W.

Fig. 3 shows the pressure profile as a function of reformer volume when the reformer is operated adiabatically and it is observed that the pressure drop is small for the radial flow reactor. When this is compared with a conventional pipe flow reactor of the same diameter as the thickness of the radial flow reactor, it is observed that there is significant pressure drop in the pipe flow reactor and it is not possible to operate the pipe flow reactor beyond 17 ml as the pressure drops to very low levels. This result is in agreement with the experimental observations of Pattekar and Kothare [15].

Fig. 4 shows the temperature profile as a function of reformer volume when 15 W of power is supplied to the reformer and it is observed that while the temperature drops from 848 to 722 K,

**Fig. 3.** Reformer pressure as a function of reactor volume.**Fig. 4.** Temperature profile for nonisothermal operation.

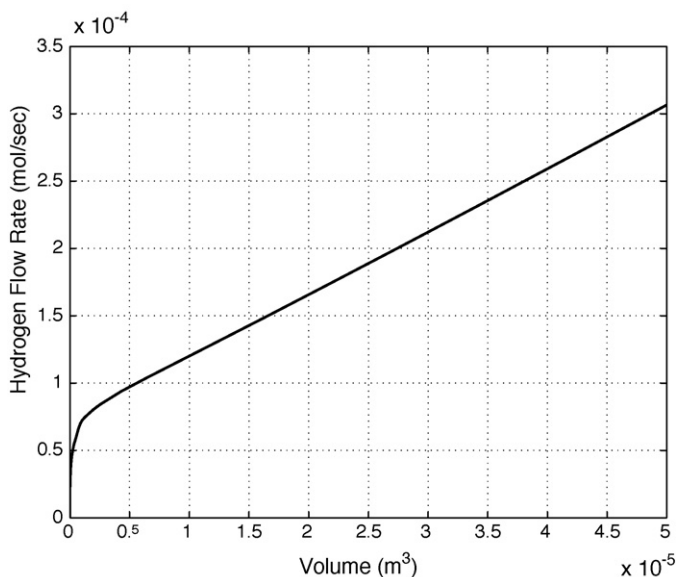


Fig. 5. Hydrogen flow rate for nonisothermal operation.

it comes back up to 800 K at the reformer outlet due to the heat input. The corresponding hydrogen flow rate profile as a function of reformer volume is shown in Fig. 5.

6. Conclusions

In this paper, an integrated model for the steady-state operation of reformer for power applications in the 20 W range was developed. Kinetic expressions from the literature were utilized for modeling the reformer. It is shown that the radial flow geometry leads to modest pressure drop. The reactor operates at a pressure of 150 kPa, a steam to methane ratio of 3 and an inlet temperature of 848 K and is able to generate sufficient hydrogen for 20 W of power. The heat duty required for the reformer is approximately 43% of the power generated. The analysis presented in this paper is based on reforming kinetics developed on Ni/MgO · Al₂O₃ catalyst. Newer catalysts based on Rh/Al₂O₃ and Rh/ZrO₂ have the potential to increase reforming reaction rates by 1–3 orders of magnitude [19,20,12]. The model developed in this paper can be easily modified for these new catalysts by replacing the rate kinetics (Eqs. (4)–(6)) by rate kinetics developed for Rh based catalysts. While

the result trends are expected to be the same, the reactor size will be reduced due to increased reaction rates.

References

- [1] R.B. Bird, L.E. Stewart, E.N. Lightfoot, *Transport Phenomena*, 2nd ed., John Wiley and Sons, 2006.
- [2] H. Chang, J.R. Kim, J.H. Cho, H.K. Kim, K.H. Choi, *Materials and processes for small fuel cells*, *Solid State Ionics* 148 (2002) 601–606.
- [3] H.S. Chu, F. Tsau, Y.Y. Yan, K.L. Hsueh, F.L. Chen, *The development of a small PEMFC combined heat and power system*, *J. Power Sources* 176 (2) (2008) 499–514.
- [4] H.W. Cooper, *Fuel cells, the hydrogen economy and you*, *Chem. Eng. Progress* 103 (11) (2007) 34–43.
- [5] H.S. Fogler, *Elements of Chemical Reactor Engineering*, Prentice-Hall, Upper Saddle River, 2006.
- [6] N.S. Kaisare, D.G. Vlachos, *Optimal reactor dimensions for homogeneous combustion in small channels*, *Catal. Today* 120 (2007) 96–106.
- [7] G. Kolb, T. Baier, J. Schurer, D. Tiemann, A. Zioogas, H. Ehwald, P. Alphonse, *A micro-structured 5 kW complete fuel processor for iso-octane as hydrogen supply system for mobile auxiliary power units. Part I. Development of autothermal reforming catalyst and reactor*, *Chem. Eng. J.* 137 (3) (2008) 653–663.
- [8] A. Kundu, J.H. Jang, J.H. Gil, C.R. Jung, H.R. Lee, S.H. Kim, B. Ku, Y.S. Oh, *Micro-fuel cells – current development and applications*, *J. Power Sources* 170 (2007) 67–78.
- [9] A. Kundu, D.H. Kim, in: T.S. Zhao, K.D. Kreuer, T. Nguyen (Eds.), *Advances in Fuel Cells Book Series*, vol. 1, Elsevier Publications, 2006, pp. 417–470.
- [10] J. Larminie, A. Dicks, *Fuel Cell Systems*, Wiley, New York, 2000.
- [11] O. Levenspiel, *Chemical Reaction Engineering*, 3rd ed., John Wiley and Sons, 1999.
- [12] M. Maestri, D.G. Vlachos, A. Beretta, G. Groppi, E. Tronconi, *Steam and dry reforming of methane on Rh: microkinetic analysis and hierarchy of kinetic models*, *J. Catal.* 259 (2008) 211–222.
- [13] National Research Council, *Meeting the Energy Needs of Future Warriors*, <http://www.nap.edu/catalog/11065.html>, 2004.
- [14] D.G. Norton, D.G. Vlachos, *Combustion characteristics and flame stability at the microscale: a CFD study of premixed methane/air mixtures*, *Chem. Eng. Sci.* 58 (2003) 4871–4882.
- [15] A.V. Pattekar, M.V. Kothare, *A radial microfluidic fuel processor*, *J. Power Sources* 147 (2005) 116–127.
- [16] B.E. Poling, J.M. Prausnitz, J.P. O'Connell, *The Properties of Gases and Liquids*, 5th ed., McGraw-Hill, 2001.
- [17] A.L.Y. Tonkovich, B. Yang, S.T. Perry, S.P. Fitzgerald, Y. Wang, *From seconds to milliseconds to microseconds through tailored microchannel reactor design of a steam methane reformer*, *Catal. Today* 120 (2007) 21–29.
- [18] *Unmanned Aircraft Systems Roadmap 2005–2030*, Office of the Secretary of Defense, U.S. DOD, 2005.
- [19] Y. Wang, Y.H. Chin, R.T. Rozmiarek, B.R. Johnson, Y. Gao, J. Watson, A.Y.L. Tonkovich, D.P.V. Wiel, *Highly active and stable Rh/MgO–Al₂O₃ catalysts for methane steam reforming*, *Catal. Today* 98 (2004) 575–581.
- [20] J. Wei, E. Iglesia, *Structural requirements and reaction pathways in methane activation and chemical conversion catalyzed by rhodium*, *J. Catal.* 225 (2004) 116–127.
- [21] J.G. Xu, G.F. Froment, *Methane steam reforming, methanation and water–gas shift. 1. Intrinsic kinetics*, *AIChE J.* 35 (1) (1989) 88–96.
- [22] M. Zafir, A. Gavriilidis, *Catalytic combustion assisted methane steam reforming in a catalytic plate reactor*, *Chem. Eng. Sci.* 58 (2003) 3947–3960.